

Disclaimer/Publisher's Note: The statements, opinions, and data contained in all publications are solely those of the individual author(s) and contributor(s) and not of MDPI and/or the editor(s). MDPI and/or the editor(s) disclaim responsibility for any injury to people or property resulting from any ideas, methods, instructions, or products referred to in the content.

Article

Different Processing of Time-domain-induced Polarisation: Application for Investigating the Marine Intrusion in the SE Iberian Peninsula

Jesús Díaz-Curiel ^{1,*}, Bárbara Biosca ¹, Lucía Arévalo-Lomas ¹ and María Jesús Miguel ²

¹ Department of Energy and Fuels, School of Mines and Energy, Universidad Politécnica de Madrid, Address: C/ Ríos Rosas 21, 28003 Madrid, Spain; j.diazcuriel@upm.es (J. D.); barbara.biosca@upm.es (B. B.); lucia.arevalo@upm.es (L. A.)

² Ministerio de Ciencia e Innovación España, Address: Paseo de la Castellana 162, 28046 Madrid, Spain; mjesus.miguel@ciencia.gob.es

* Correspondence: j.diazcuriel@upm.es

Abstract: This study presents the developments regarding the time-domain-induced polarisation method, as a supporting tool for resistivity soundings during investigations of coastal detrital aquifers that are salinised by marine intrusion. The interpretation of resistivity measurements in such aquifers, which have variable hydrochemistry and lithology, involves uncertainties owing to the presence of low-resistivity lithologies, such as clays. To reduce these uncertainties, the use of other geophysical parameters is necessary; hence, this study focuses on induced polarisation, since it can be measured simultaneously with resistivity. In detail, we propose the determination of induced polarisation using 1D techniques, while developing a different algorithm for processing the induced polarisation data. The aim is to extend the results of this phenomenon, using instead of chargeability, the concepts of polarisability and decay time, which are extracted from the decay curve, given that they represent more intrinsic properties of the various analysed subsurface media. We present results obtained by applying this methodology to a Quaternary aquifer of the Costa del Sol in the SE Iberian Peninsula (in the province of Almería) during two different campaigns, one before and one after winter (i.e., in October and February, respectively). The results reveal the position of the saline front during each campaign, while reflecting the seasonal movement of the marine intrusion.

Keywords: marine intrusion; induced polarisation; polarisability; decay time

1. Introduction

The geological and lithological characteristics of a formation assigned solely based on resistivity can be partially ambiguous when media with similar resistivities coexist. Besides the lithological differences, the resistivity values of geological formations depend on a large number of petrophysical variables in these media as well as the hydrochemical characteristics of the formation water. Many 1D geoelectric prospecting studies often consider that an adequate geological interpretation can only be achieved based on previous knowledge of the area; however, this consideration may not be appropriate as a general criterion.

The intrinsic parameter that best discriminates the media from a geoelectrical point of view is the formation factor ($F = \rho / \rho_w$, where ρ is the resistivity of the medium and ρ_w is the resistivity of the pore fluid); hence, the hydrochemical characteristics of the pore fluid strongly affect the resistivity of the medium. For example, an aquifer composed of granular lithologies can have resistivities very similar to those of clays ($\sim 10 \Omega \text{ m}$) when the formation fluid has a conductivity of a few tenths of S/m, corresponding to that of a freshwater/seawater transition fluid (interface). However, this ambiguity can be reduced by using more than one geophysical parameter.



The induced polarisation (IP) survey method allows the acquisition and measurement of a second parameter with the same electrode arrays as those used for obtaining the resistivity. This method is based on the IP phenomenon discovered by Schlumberger in 1920 [1,2] and has been the product of continual development [3-6]. The method involves analysing the electrical response of the terrain to the variation of a certain generated electric field, either by measuring over time the field—i.e., the potential—that remains in the medium when the applied current is cancelled (time-domain TDIP) or by measuring the electrical response of the terrain when the frequency of an alternating current varies (frequency domain SIP).

In time-domain measurements, two parameters can be distinguished according to the historical evolution of this method. Initially, the objective was to register the potential immediately after cancelling the current injection, thereby establishing the polarisation capacity of the medium through the relationship between the potential measured just before cancelling the applied field V_P (primary potential) and the potential measured just after cancelling the external field V_S (secondary potential) ([7]; Eq. 1):

$$m = \frac{V_S}{V_P} \cdot \ln \left(\frac{mV}{V} \right) \quad (1)$$

However, partly because it is difficult to measure the established V_S , it is common practice to measure the decay of the voltage over time, which is typically measured in successive time windows, while obtaining the value of m using the following expression [8]:

$$m = \frac{\int_{t_1}^{t_2} V_S(t) \cdot dt}{(t_2 - t_1) \cdot V_P} = \frac{\bar{V}_S}{V_P}, \quad (2)$$

where $V_S(t)$ is the potential value measured over time after cancelling the primary potential, and $(t_2 - t_1) = \Delta t$ is the integration interval. Thus, the value \bar{V}_S obtained through this integral is attributed to the secondary potential.

Although the term *polarisability* was also being used initially, the term *chargeability* prevailed in time and is assigned indistinctly to the parameter obtained by either Eq. (1) or Eq. (2). Fiadanca et al. [9] differentiated the parameters obtained by Eqs. (1) and (2) by calling them *intrinsic chargeability* and *integral chargeability*, respectively. The main limitation that the authors identified regarding Eqs. (1) and (2) was that they may provide decay curves with the same chargeability, but different polarisabilities and decay times, suggesting that they correspond to different IP sources (Fig. 1). Because IP decay curves do not necessarily correspond to mono-exponential behaviour, the decay time reflected in Fig. 1 corresponds to $V_S(0)/e$. For this reason, in this study, the term *chargeability* refers to the value obtained by Eq. (2) and *polarisability* P refers to the value obtained by Eq. (1), modified to consider only the part of the secondary potential that corresponds to the $V_{IP}(t=0^+)$ polarisation effect.

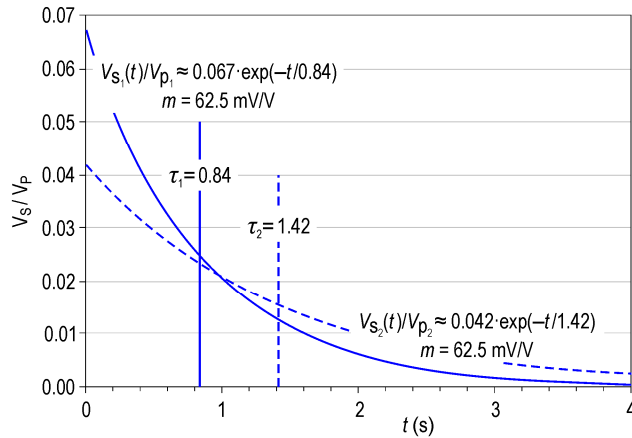


Figure 1. Example of two decay curves with the same chargeability, but different polarisabilities and decay times.

Some studies have focused on the decomposition of the decay curve at each depth of investigation into a sum of different exponentials. In this study, we present an alternative decomposition involving dividing the decay curve into only three exponentials. One of the three exponentials corresponds to the electromagnetic induction effect, another represents the IP decay due to the different layers influencing each depth of investigation, and a third corresponding to a residual potential found in many of the cases studied.

Regarding the IP in the frequency domain, owing to the increased operability and electronic ease, there has been greater development of these methods. This development began with the investigation of the frequency effect (FE) based on the resistivity variation for two highly differentiated frequencies $\omega_1 \gg \omega_2$ given by Eq. (3):

$$FE = \frac{|\rho(\omega_2)| - |\rho(\omega_1)|}{|\rho(\omega_1)|} \cdot 100\%. \quad (3)$$

This frequency effect has often been calculated by considering $\omega_2 = 0$, i.e., $\rho(\omega_2) = \rho_{DC}$ [10]. In the model defined by Cole and Cole [11], the complex resistivity for frequency ω_k is given by Eq. (4) [12]:

$$\rho(\omega_k) = \rho_0 \langle 1 - m \{1 - [1 + (i \cdot \omega_k \cdot \tau)^c]^{-1}\} \rangle, \quad (4)$$

where ρ_0 is the resistivity in direct current, m is the chargeability, τ is the time constant of the IP, and c is the frequency exponent (slope on the logarithmic scale of both sides of the phase curve) with a maximum value of 1. Regarding the relationship between the two domains, which was introduced by Cole and Cole [11], different researchers have introduced different expressions established by different researchers [13-14], including an expression accounting for the electromagnetic coupling (EM) effects [15]. Thus, several studies used the IP method in the frequency domain and its relation to the time domain, thereby determining different time constants depending on the petrochemical and hydrochemical characteristics of the subsurface. Pelton et al. [12] conducted an exhaustive study of the electrical response of metallic formations and found typical frequency-exponent values ranging from 0.1 to 0.6, with a mean value of 0.25; they also conducted an analysis of the spectral behaviour of the studied reservoirs, thereby determining different values for τ . Given the above-mentioned terminological differentiation, the logical interrelation of IP in the time and frequency domains is more closely linked to chargeability.

After establishing the importance of IP in the time domain, this study introduces in detail a way to process the TDIP decay curves, while providing the value of the $V_{IP}(t=0^+)$ polarisation potential with the aim of differentiating the presence of clay levels through geoelectric soundings conducted in coastal detrital aquifers. The inclusion of such clay levels, which have higher polarisability values than those of granular strata, improves the inversion of resistivity soundings in which this presence was not considered [16] and

elucidates the marine intrusion progress. The proposed methodology was applied to a case of marine intrusion and eventually provided the seasonality of the salt wedge.

One aspect of this study that should be noted is the choice of 1D techniques. Currently, most research teams using electrical prospecting techniques have opted for 2D or 2D+1 techniques with higher lateral resolution. In this respect, it is worth mentioning the study of Höning and Tezkan [17], who conducted an exhaustive analysis involving tomographic inversion (2D for 1D inversion and 3D for 2D inversion), while considering τ and c for cases with $m > 0.15$.

Regarding, the IP measurement, there are certain drawbacks regarding the tomographic profiling measurement. First, the use of non-polarisable electrodes for conducting potential measurements is not suitable for the current circuit; this is only possible with some of the existing tomography systems or with the use of specific measurement arrays that differentiate the injection positions from the potential-measurement positions. Second, unlike the multi-conductor cables used in tomographic measurement equipment, obtaining higher-quality measurements requires the use of separate cables for current and potential circuits [18]. Third, when investigating coastal aquifers in countries with high proportions of buildings and/or agricultural plots, tomographic measurements are hindered, with the presence of fences and small buildings preventing the use of cables with fixed connectors at certain distances and requiring the use of single-conductor cables with highly variable lengths for different electrode positions.

Marine intrusions that have the greatest repercussions on groundwater exploitation have high spatial extensions; this makes them appropriate for conducting 1D studies. The aim of the project to which these studies belong was to evaluate the temporal evolution of the freshwater/saltwater interface by conducting successive low-cost campaigns, thereby also conditioning the choice of 1D studies with a reduced number of measuring arrays. In relation to 2D studies, the exhaustive work of Ogilvy et al. [19] is worth mentioning, since they developed an automated measurement system (ALERT) for monitoring, among other phenomena, the marine intrusion advance and its effects on the underlying Quaternary aquifer.

2. Background

The IP prospecting method was initially called over-voltage and became very important in the 1950s for locating metal deposits [20-23]; its use for exploring clay strata, characterising petrophysical properties, and investigating groundwaters of different salts concentrations has since then increased.

The initial identification of the influence of clays on the IP responses resulted in several studies on various related theoretical aspects [7,24], which was followed by multiple studies on their application in different environments [23-28], others studied the specific characteristics of the responses of clays [29-31]. Relationships between the IP parameters and different granulometric characteristics of different media were also established. On the one hand, Börner et al. [32] and Slater and Glaser [33] determined different empirical relationships between specific pore-surface areas and IP results; on the other hand, several studies demonstrated a clear relationship between the decay time, derived from the Cole-Cole model from frequency-domain measurements, and the pore size of formation. Titov et al. [2], Scott and Barker [34], and Binley et al. [35] presented empirical relationships established between the time constant and minor grain size.

Besides the lithological characteristics, the hydrochemical characteristics can also result in ambiguities in the IP values of different formations in the subsurface. However, the weight of the hydrochemical characteristics is different from those of the lithological and petrophysical characteristics [36], thereby reducing the ambiguities when comparing the resistivity and polarisability of a certain medium. Consequently, many studies have tried to confirm the relationship between IP and the hydrochemical characteristics of formation [37-41]. Such ambiguities occur when studying areas with fully or partially salinised aquifers, which can be confused with clay levels if only resistivity values are available. The

ambiguities can be reduced or avoided through IP measurements, which are widely used in studies on marine intrusions and the salinisation of aquifers [42-49]. However, IP measurements have also been applied in recent studies of organic fluid pollution with nonaqueous phases, with the results being rather variable and, in some cases, unsatisfactory [50-56].

2.1. Influence of electromagnetic (EM) coupling

As with any measure in a variable electric field, EM induction effects in the subsurface may also be included when conducting IP measurements. Depending on the array used and, in our case, the study time, the relative proportions of the effects may vary. For this reason, the arrays used for IP measurements are usually linear and the time windows for measuring the IP decay curve are between 0.25 and 2.50 s. Nevertheless, it is necessary to eliminate the possible influence of EM effects on the IP measurements.

The separation of IP effects from EM coupling has been performed more extensively in the frequency domain, where much shorter decay times are considered based on the transfer function.

Luo and Zhang [57] used an equivalent '2nd order' model to describe the presence of EM coupling in the IP by adding another term to Eq. 4:

$$\rho(i \cdot \omega_k) = \rho_0 \left\{ 1 - m \{ 1 - [1 + (i \cdot \omega_k \cdot \tau)^c]^{-1} \} - m' \{ 1 - [1 + (i \cdot \omega_k \cdot \tau')^c]^{-1} \} \right\}. \quad (5)$$

This main theoretical drawback of this technique lies in the variation of resistivity with frequency, while its application in the field is limited by induction phenomena and residual potential, resulting in nonzero signal background.

2.2. Measurements in the time domain

By studying the decay curve in the time domain, the different effects appearing in it (e.g., induction, polarisation, coupling, noise, etc.) can be more easily discriminated and separated.

The most detailed mathematical process for decomposing the decay curve into a sum of exponentials is the Laplace decomposition. Although this decomposition can result in a very large number of exponentials corresponding to differential decay-time increments, for IP decay curves the number of exponentials should be limited to the number of study (time) windows used during the measurement. One of the main advantages of the Laplace decomposition is the identification of areas within the integration period with higher occurrence of errors or noise, which in the frequency domain would appear as part of the total spectrum. During analysis of the complete curve, the sum of exponential functions fitted to the points may not sufficiently represent some of them, especially if measurements have been performed with a low V_p value; for these 'noisy' bands, specific criteria can be adopted. Overall, it is worth remembering that using filters for noninfinite signals involves limitations.

Other studies have conducted the same type of decomposition in different manners. Luo and Zhang [57] proposed the decomposition of the decay curve $E(t)$ into a wide series of decreasing exponentials $A_n \cdot \exp(-\alpha_n t)$, corresponding to the different contributions to the total polarisation of the different subsurface formations:

$$E(t) = E_0 \left[1 - \sum_n A_n \cdot \exp(-\alpha_n t) \right], \quad (6)$$

where $E_0 = \lim_{t \rightarrow 0} E(t)$.

Some authors have considered specific coefficients and time constants as functions of different lithologies and different proportions of dissolved ions present in formation water. Thus, Xiang et al. [58] considered for the case of 20% pyrite and 80% andesite in 5% 0.01 N ClNa water the following coefficients (Eq. 7):

$$E(t) = E_0 [1 - 0.29 \exp(-5.7 \cdot t) - 0.11 \exp(-40 \cdot t) - 0.10 \exp(-300 \cdot t)]. \quad (7)$$

However, the coefficients used to separate the EM coupling effects from the IP are defined in the direct solving, but not inversely, for the different decay curves

Tong et al. [59] conducted laboratory experiments for which the precision of the measurements allowed the relaxation-time spectrum to be considered as the weight coefficients of each of the exponentials into which the decay curve can be decomposed (Eq. 8):

$$y(t) = \frac{V(t)}{V(0)} \int_{t_{min}}^{t_{max}} V_N(\tau) \exp\left(\frac{t}{\tau}\right) d\tau. \quad (8)$$

Apart from a complex acquisition of measurements over a large number of time windows during field surveys, this division requires almost total absence of noise in the measurements. If the measurements are not sufficiently accurate, the Laplace decomposition may produce a sum of exponentials that do not represent subsurface stratification.

Another method for decomposing the polarisation curve into a sum of two decaying exponentials involves applying the stretched exponential relaxation function [60], although the choice between the two options depends on the physics of the process itself. Some authors have applied this methodology for the IP analysis as an alternative to the Cole–Cole model [61–62].

In this study, we present an alternative decomposition involving dividing the decay curve into only three exponentials: one exponential corresponding to the EM effect, another representing the IP decay due to the different layers influencing each depth of investigation, and a third corresponding to a residual potential that is evident in each case. In our opinion, the latter should also be previously removed in the Laplace decomposition, if stratigraphically meaningful results are to be obtained.

3. Materials and Methods

One of the main challenges in the application of IP in the time domain is to obtain as reliable data as possible in each time window. Most equipment does not have the possibility of separate stacking of responses for each time window. This is particularly relevant if we consider that the use of each window implies the inclusion of noise of different frequencies. The equipment used in this study did have this possibility, as well as allowing a higher power-supply intensity than that supported by another current DC equipment.

The methodology for processing decay curves is another key issue in the application of IP in the time domain. The main methodological contribution of this study is the proposal of such processing involving dividing the IP curve into three ‘potentials,’ one potential with a short time period corresponding to the EM effects, another with an intermediate time period corresponding mainly to the IP effects, and a third residual one with much higher time constant ($\rightarrow \infty$) that is different from those theoretically considered. The reason for including a residual potential is the presence of an electrode potential which, although time-varying, can be considered constant in conventional measurement periods in IP studies. Although this effect has been minimised using non-polarisable electrodes (Fig. 2), its elimination is indispensable and relatively easy in the treatment of time-domain IP.

3.1. Data acquisition

The instrumentation consisted of a Scintrex TSQ-3 (3 kW) square-wave transmitter with 4 s charging pulses connected to two steel electrodes. With the Scintrex IPR-10A receiver, measurements were obtained in six 520-ms time windows between 260 and 3380 ms (average times from 520 up to 3120). For the ΔV measurement, we used flat non-polarisable electrodes from Geotron, which consisted of semi-permeable porous vessels filled with a supersaturated copper sulphate solution (Fig. 2). These electrodes were used to minimise the electrode polarisation effects, which are typically present in IP

measurements. Resistivity and IP measurements were conducted simultaneously. The use of non-polarisable electrodes and separate current and potential cables, as mentioned in the introduction, allowed measurements of satisfactory quality. For the same reason, we made sure to place the potential cables perpendicular to the current cables.



Figure 2. (a) Scintrex TSQ-3 equipment and IPR-10A receiver. (b) Fat non-polarisable electrodes with CuSO_4 .

3.2. Analysis of the decay curves

As mentioned before, the processing of the decay curves involves dividing them into three 'potentials,' one potential with a short time period corresponding to the EM effects, another with an intermediate time period corresponding mainly to the IP effects, and a third residual one with much higher time constant ($\rightarrow \infty$) that is different from those theoretically considered. In practice, with a fit to the sum of the first two exponential functions, plus a residual value towards which the decay curve is asymptotic, the phenomenon can be considered sufficiently described, with the precision obtainable in the field (Eq. 9):

$$V_{s(t)} = V_{0EM} \cdot e^{-t/\tau_{EM}} + V_{0IP} \cdot e^{-t/\tau_{IP}} + V_R, \quad (9)$$

where the first term is mainly due to the inductive response of the medium and the second term is due to the depolarisation of the medium. We note that the time windows used in IP do not adequately estimate the initial induction potential; therefore, the V_{0EM} value is only analysed with regard to the decomposition of the decay curve. The reason for including a residual potential V_R is the presence of a potential difference between the electrodes, which can be considered constant in conventional measurement times in IP studies. In fact, V_R showed differences between successive measurement points or stations of each sounding, without stratigraphic justification. Although this effect has been minimised by using non-polarisable electrodes (Fig. 2), its elimination is necessary and relatively easy in the treatment of IP in the time domain.

Moreover, even when the removal of EM electromagnetic and residual effects is highly reliable, the remaining curve still includes the effects of two factors working in tandem: the salinity of the formation water and the petrological characteristics of each stratum. For this reason, two different parameters were obtained from the IP curve: polarisability P (the extrapolated value of the polarisation potential at $t = 0^+$ divided by the potential just before that time, $t = 0^-$) and the period or decay constant τ_{IP} of the curve. In this study, we considered that the petrology of the medium mainly affects the decay period, whereas the mineralogical characteristics affect particularly the polarisability. As mentioned above, the measurements of polarisability and decay time represent a clear advantage over the measurement of chargeability within a given time window (although this is currently the most common procedure). It is easy to see that two different decay curves can have the same chargeability, measured in a single window; however, analysis of the complete decay curve shows that both the cut-off point at $t = 0^+$ and the decay period are different, while representing more intrinsic values of the rock (Fig. 1).

The key of the decomposition, as shown in Eq. (9), is twofold: On the one hand, the decomposition of a gradually decreasing signal into a sum of an exponential and a constant value does not represent any remarkable complexity; on the other hand, the decay times τ_{IP} and τ_{EM} are intrinsically different. Typically, the polarisation time varies between one and several seconds, whereas the induction time is a few tenths of a second long. In this study, the decomposition method involved performing a series of approximating iterations, which required an initial decomposition to avoid convergence problems. Thus, the steps for the decomposition of the decay curve were as follows.

Initially, by minimising the approximation error of the measured decay-data curve (V_n, t_n) to a simple exponential plus a constant potential, $V_{S(t)} = V_0 \cdot e^{-(t/\tau)} + V_{R0}$, we obtained the value of the cut-off potential V_{0T} and verified that the obtained value coincided (i.e., $\pm 2\%$) with that obtained by determining the residual potential minimising the variance between successive point-to-point decays. Then the next steps were:

(1) The approximation of the decay-data curve of a modulated exponential is given by Eq. (10):

$$V_{S(t)} = V_{0M} \cdot e^{-(t/\tau_M)^m}, \quad (10)$$

through an iterative process, where the variable is the modulation exponent m .

(2) We generated a curve equal to the sum of a simple exponential plus a constant value; thus, by using the average decay constant τ_{MED} of the successive point-to-point decays, the integral is the same as that of the original data curve (Eq. 11).

$$V_{S(t)} = V_{0\Sigma} \cdot e^{-(t/\tau_{MED})} + V_{R2}, \quad \sum V_n \cdot \Delta t_n = \int V_{S(t)} \cdot dt. \quad (11)$$

After analysing the correlation coefficients with 28 initial decay-curve cases, we found that the cut-off potential of Eq. (9) is equal to that of Eq. (11), i.e., $V_{0EM} + V_{0IP} + V_R = V_{0\Sigma} + V_{R2}$, and that $V_{0EM} + V_{0IP} = 1.16 \cdot V_{0M}$. We also found that the difference between the cut-off potentials corresponding to the two equations, V_{0M} and $V_{0\Sigma} + V_{R2}$, were highly correlated (i.e., $R^2 = 0.98$) with the residual potential. Thus, the minimum deviation relationship providing the residual potential was given by Eq. (12):

$$V_R = (V_{0\Sigma} + V_{R2}) - 1.16 \cdot V_{0M}. \quad (12)$$

This decomposition was found to be effective for all the decay curves analysed in the campaign, except in one case (the first station of sounding P1-N), which had a modulation exponent of 0.55; therefore, the value of 0.6 can be considered as a safety criterion for the modulation exponent, the maximum value obtained for the modulation exponent was 1.0 (corresponding to $V_R = 0$).

(3) By subtracting the residual potential V_R , a $V_{IPEM}(t)$ curve is obtained, in which the separation between the two remaining exponentials is subtler. For this separation, after obtaining an initial potential V_{01} by fitting to a modulated exponential $V_{IPEM}(t) = V_{01} \cdot e^{-(t/\tau_1)^n}$, and a decay period τ_2 by approximating to a simple exponential $V_{IPEM}(t) = V_{02} \cdot e^{-(t/\tau_2)}$, the cut-off potential and the polarisation period were obtained by approximating the expression Eq. (13):

$$V_{IPEM}(t) = (V_{01} - V_{0IP}) \cdot e^{-\frac{t}{\tau_{EM}}} + V_{0IP} \cdot e^{-\frac{t}{\tau_{IP}}}. \quad (13)$$

We took the following as the initial iteration values: $V_{0EM} = V_{0IP} = \frac{1}{2}V_{01}$, $\tau_{IP} = \tau_2$, and $\tau_{EM} = 0.33 \cdot \tau_2$. By taking into account that $V_{IPEM}(0) = V_{0EM} + V_{0IP} = V_{01}$, we obtained the values of V_{0IP} and τ_{IP} , and thus the final polarisation curve (Eq. 14):

$$V_{IP}(t) = V_{0IP} \cdot e^{-\frac{t}{\tau_{IP}}}. \quad (14)$$

In this iterative process, the relative errors were very low (i.e., between 0.1 and 1.5%) with a difference related more to the small curvature changes than to the difference between the model and the $V_{IPEM}(t)$ values; therefore, the similarity in the second derivative was adopted as the iteration criterion. Figure 3 shows an example of the two curves of V_{01} and

V_{02} obtained with very low error for the data of a decay curve, which nevertheless show a clear difference in curvature, such that the ratio between the two should be centred around 1.

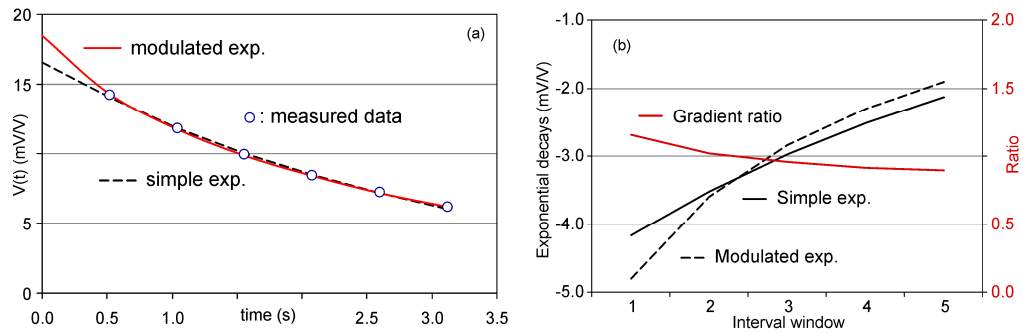


Figure 3. (a) Approximation exponentials. (b) Derivative curves and their ratios.

Using the described procedure, for each AB position in each sounding, the decay curves were modelled to obtain the values of V_{0IP} and τ_{IP} . Figures 4a and b show two examples of the decomposition of the decay curves at one of the case-study points. In the first example, the electric field is mostly above the freshwater/saltwater interface, showing a clear positive coupling; in the second example, where a larger fraction of the electric field penetrates below the marine interface, V_{0EM} and V_{0IP} decrease, showing an apparent induction opposite to that of the created field.

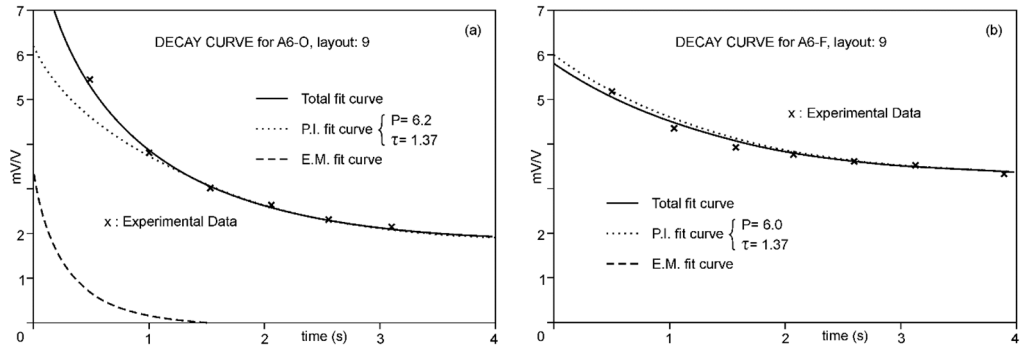


Figure 4. (a). Decay curve of sounding A6-O, station 9. (b). Decay curve of sounding A6-F, station 9.

After analysis of the results, we found that the mean value of τ above and below the interface ranged from 1.4 to 1.2 s; based on this small difference, we dismissed the use of decay time in this study.

3.3. VES-IPS inversion

The apparent-resistivity data of each VES-IPS were interpreted by semi-automatic fitting of a curve generated from an initial model using the software developed by our research group. The method used for generating this curve is based on the convolution of the thicknesses and resistivities using the filter of Ghosh [63].

Furthermore, the apparent-polarisability data were interpreted using the same methodology by varying the mathematical process that generated the curves. For this purpose, we adopted the expression proposed by Seigel [7] and modified by Roy and Poddar [64] for n layers:

$$P_a(r) = \frac{\rho_a(r)(\rho_j + P_j \cdot \rho_j) - \rho_a(r)(\rho_j)}{\rho_a(r)(\rho_j)}; (j = 1, \dots, n), \quad (15)$$

where: $\rho_a(r)$ is the apparent resistivity for the half-space of the r electrodes, ρ_j is the resistivity of layer j , P_j is the polarisability of layer j .

The program developed starts from the digitised data at progressive distances from 1.5 to 220.0 m, so that six points are used in each logarithmic cycle.

4. Application for investigating the marine intrusion in the SE Iberian Peninsula

4.1. Overview of the study area and field survey

The investigated aquifer is close to the mouth of the Río Verde (Almuñécar) in the province of Granada, located at the SE Iberian Peninsula (Fig. 5); it comprises loose alluvial conglomeratic and sandy materials, with more abundant silty clay intercalations towards the coast. Below the siliciclastic basin is an impermeable substratum of schist and/or carbonate type. The overexploitation of this area is known from historical hydrochemical data [65]. During the summer period, this overexploitation of water generates an inversion of the subterranean hydraulic gradient, giving rise to a marine intrusion, which for the same reason allows desalination during the recharge period [66]. The alteration of these processes has been observed for decades.

We performed four vertical electrical parametric soundings and 18 vertical electrical and IP soundings (VES-IPS); their locations are shown in Fig. 5. In all cases, we used a Schlumberger array, with interelectrode distances from 1.5 m to a final distance (AB) of 440.0 m, to obtain 10 points per logarithmic cycle. The fieldwork began with a first campaign of four parametric soundings (at each point, two soundings were conducted by placing the electrodes along two perpendicular directions) to evaluate the influence of the layer dip. This means that it was unknown whether the 1D inversion model was applicable or, conversely, the dip of the strata produced very different inversions. Results indicated that the 1D inversion was sufficiently valid. Subsequently, we conducted two temporally separated campaigns with nine VES-IPS, one in October (pre-winter) and one in February (post-winter), to assess the seasonal advance of the marine intrusion.

Despite the combination of structures, particularly the abundance of greenhouses, it was possible to conduct a line of soundings that provided a reliable delineation of the marine-intrusion interface. In addition, by accessing some piezometers installed in the area, we were able to cross-check the results of the electrical soundings.

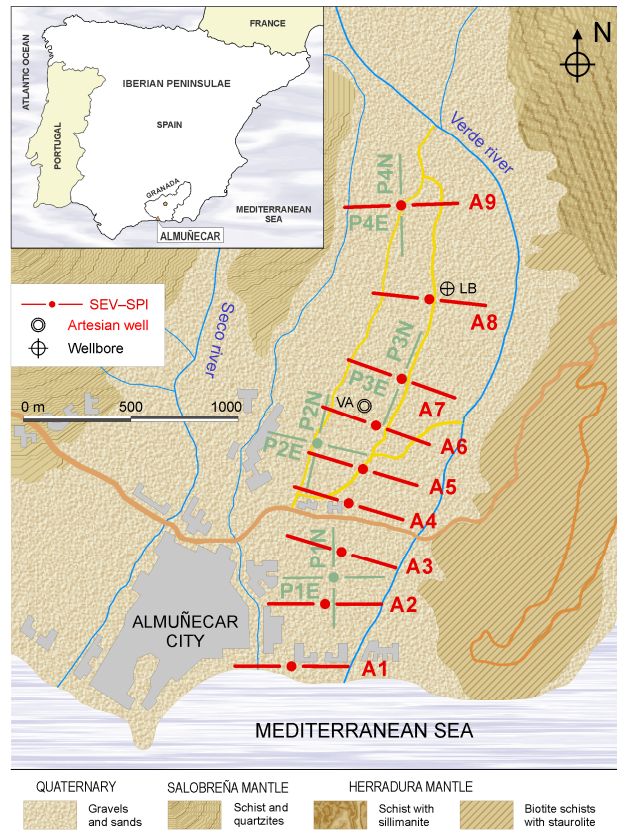


Figure 5. Location of the study area, sketch of the locations of the soundings, and geology of the area.

In the Almuñécar aquifer, a network of conductivity/temperature sensors was installed on 15 piezometers that were distributed along the axis of the aquifer; the instrumentation was used to contrast the degree of advance of the saline front in each campaign (before and after the winter) [67].

4.2. Analysis of the VES-IPS results

Figures 6 to 11 present some of the results of the VES-IPS curves obtained during the two campaigns, together with the models obtained after inversion. Given the influence on the final inversion result of the previous model required, in the following, we describe some issues that have been considered to establish in these previous models.

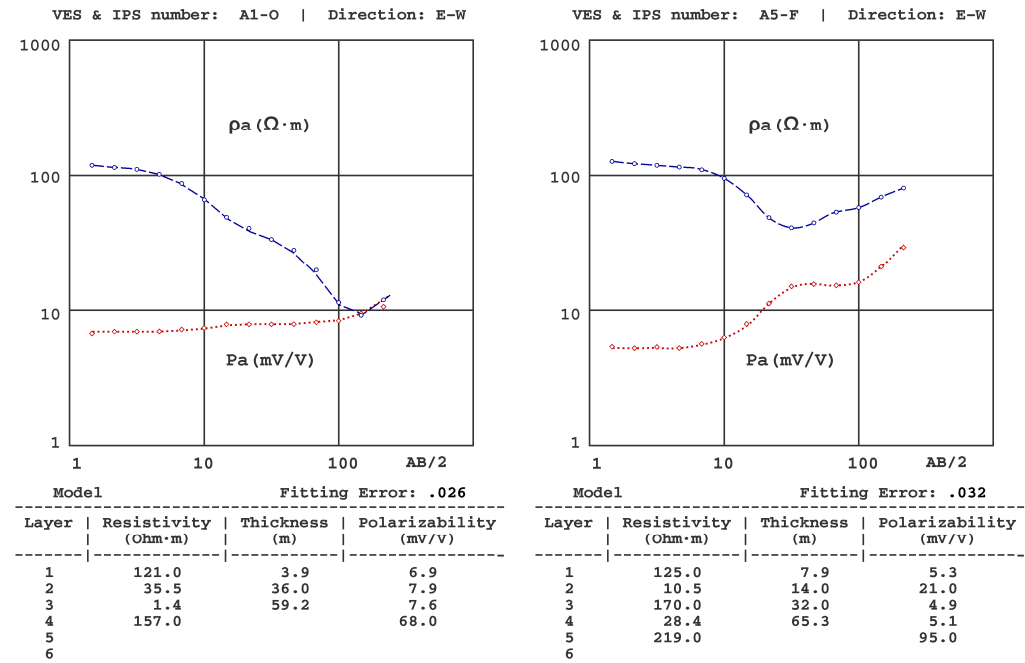


Figure 6. Results of the (a) A1-O VES-IPS obtained before winter and (b) A5-F VES-IPS obtained after winter.

1) The presence of different resistivity levels was considered when establishing the polarisability levels, despite the SIP curves not showing equally significant differences. We note that the initial polarisability value assigned to the clay levels was obtained from the results of the A5-O sounding (Fig. 7a), given that this was the one where the clays were closer to the surface and, therefore, allowed a more precise determination of their polarisability (~20 mV/V).

2) Following Eq. (15) [7], the resistivity gradient significantly affected the polarisability values, with the gradients of the IPS depending not only on the difference in P values between layers, but also on the difference in resistivity. One of the effects of this interrelationship was the possibility of sharp changes in the IP curve, such as the one for the A5-O sounding and from a sounding conducted in another basin on the same coast. In principle, we could assume that there was some error in the data collection (despite repeatedly verifying these results), but the inversion showed that the theoretical model corroborates such an abrupt change. In this regard, we note that we have found similar cases in unpublished marine intrusion work (see Figs. 7a and b).

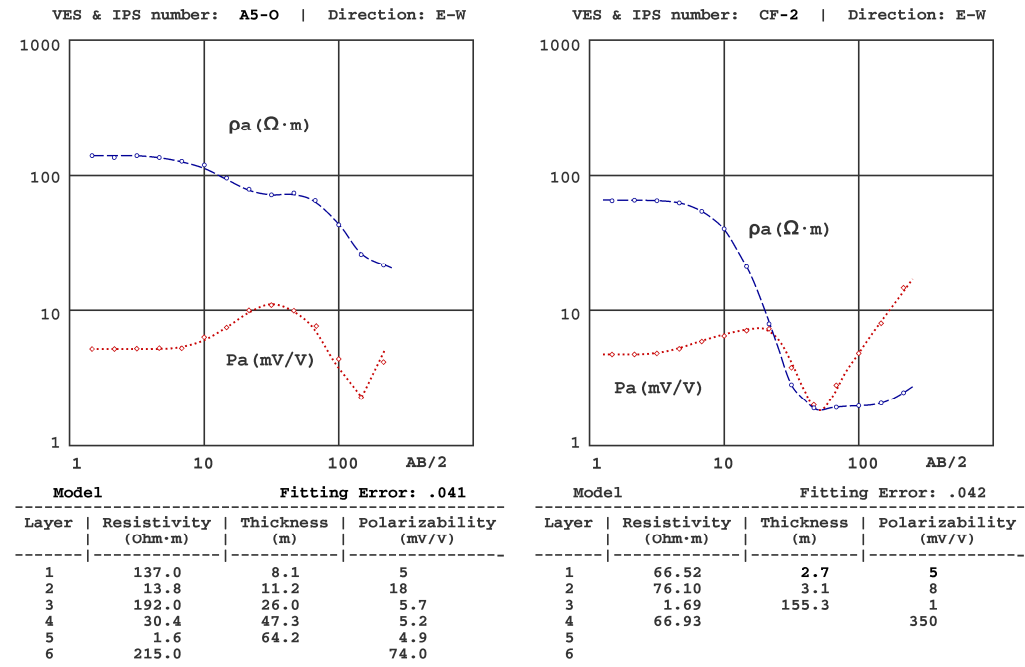


Figure 7. Results of the (a) A5-O VES-IPS obtained before winter and (b) of the CF2 VES-IPS conducted in another basin in the same region.

3) Although the convenience of a greater final AB distance became apparent from the field measurements and more evident after the inversion of the soundings, such an increase could not be achieved because of the difficulty of progressively crossing more crop farms. In any case, the resistivity of the schists was well established in VESs further in the north. However, because of the distribution of polarisability values with depth, the polarisability value was well established from both A4-O VES-IPS and A4-F VES-IPS (Fig. 8), especially during the marine-intrusion regression campaign conducted in October (before winter).

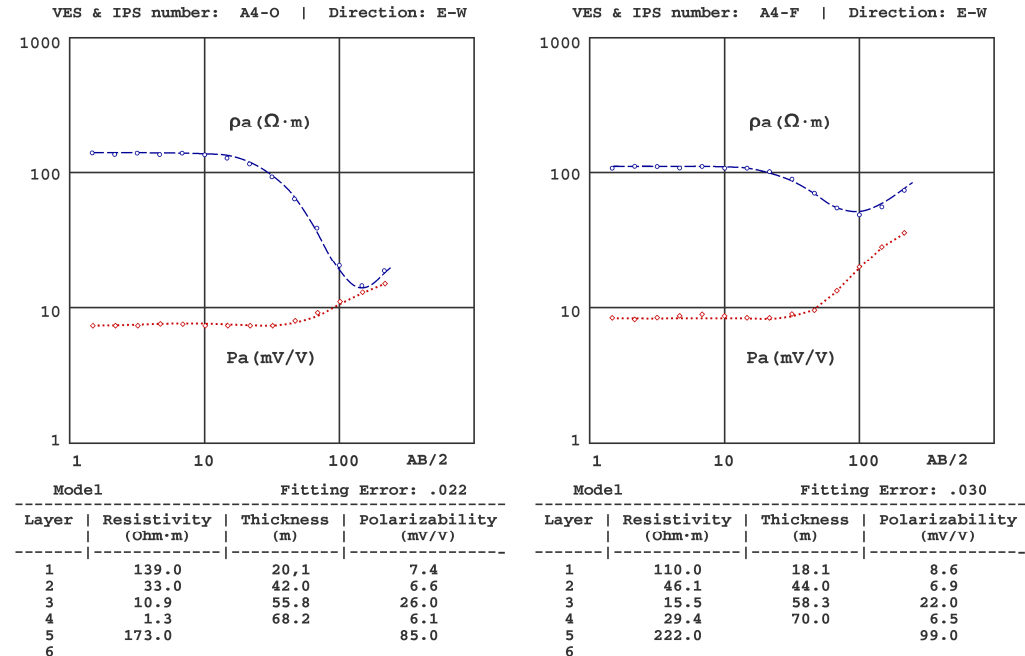


Figure 8. Results of the (a) A4-O VES-IPS obtained before winter and (b) A4-F VES-IPS obtained after winter.

Figure 9 shows VES-IPS results with clear differentiation of the geoelectric levels; however, the values of the last level are somewhat undefined (in A8-O VES-IPS and A9-O VES-IPS, the polarisability is well-defined). Fortunately, the inversion provided values more accurately, given its influence on the behaviour of the final part of the VES-IPS curves.

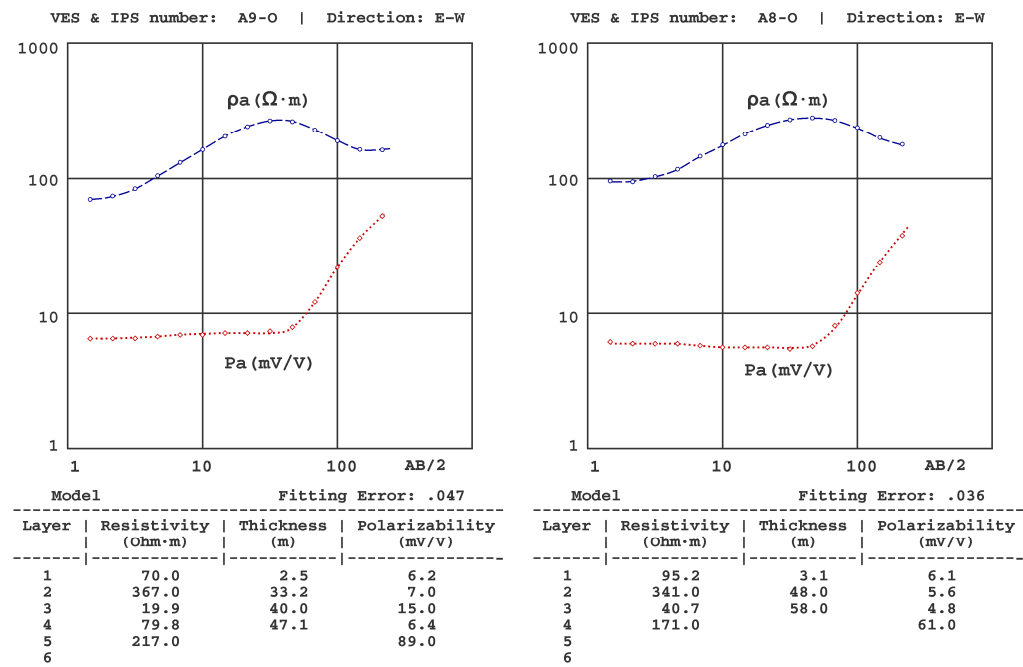


Figure 9. Results of the (a) A8-O VES-IPS and (b) A9-O VES-IPS, both obtained before winter, showing a clear differentiation of the geoelectric levels and an apparent uncertainty of the values of the deeper layers.

4) For the VES-IPS inversion, it was necessary to use models with an intermediate resistivity layer between the layer saturated with freshwater and the layer saturated with saltwater. In A3-O VES-IPS (Fig. 10), the resistivity of this layer was well established, with a value of $9 \Omega\cdot\text{m}$; however, this does not imply that this value should be maintained throughout the section obtained in each survey. In some cases, a progressively decreasing resistivity model could have been used, but this would unnecessarily complicate the VES modelling.

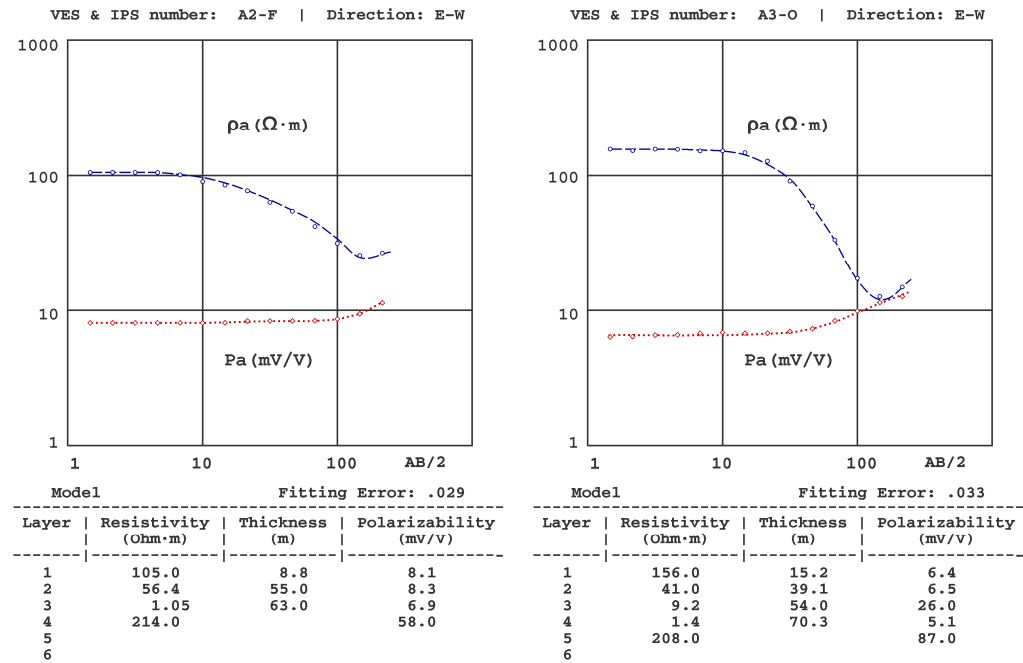


Figure 10. Results of the (a) A2-O VES-IPS and (b) A3-O VES-IPS, both obtained before winter.

5) The lack of accuracy in deeper levels (i.e., before reaching the schist substrate) with different resistivities and reduced thicknesses must be considered. In some cases, the subdivision into distinct levels is strongly supported by the differentiation shown by the IPS curves. Figure 9 shows the A9-O VES-IPS curves, in which the possibility of the previous model predicting the value of the geoelectric level corresponding to the gravel/conglomerate interface with that interstitial fluid has been reduced.

6) The inversion would produce important differences in the obtained distribution of thicknesses and/or resistivities if the initial models did not consider the presence of the clay layer. As an example, Fig. 11 shows the inversion of the A5-F sounding without consideration of the clay layer, in which the greatest difference occurs in the depth of the substratum, which is 96 m, as opposed to 65 m obtained in the inversion of the same sounding with consideration of the clay layer (Fig. 6).

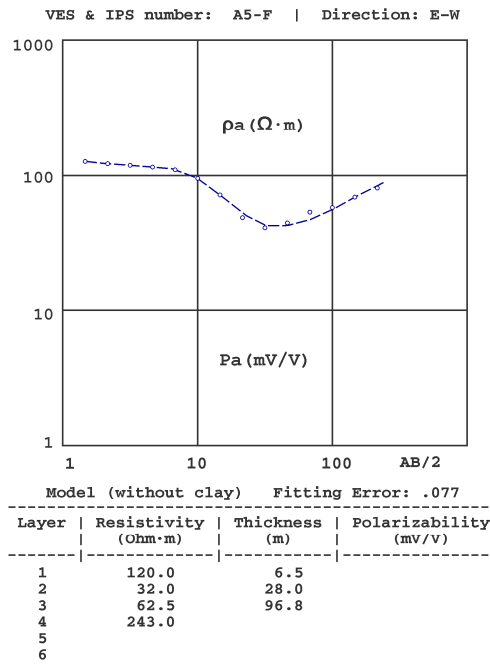


Figure 11. Results of the A5-F VES-IPS obtained after winter.

By comparing the results of the lithological columns in the two boreholes located very close to the delineated profile with those of the geoelectric soundings, we observed that the latter showed a somewhat more differentiated subdivision of the subsoil, determining up to six differentiated geoelectric levels. Table 1 shows the final inversion results obtained in the VES-IPS set before winter.

Table 1. Resistivity and polarisability values in October (before winter) obtained with VES-IPS inversion.

A1			A2			A3			A4			A5			
z	Q	P	z	Q	P	z	Q	P	z	Q	P	z	Q	P	
3.9	121	6.9	9.5	132	6.4	15	156	6.4	20	139	7.4	8.1	137	5.1	
36	35.5	7.9	41	47.9	7.0	39	41	6.5	42	33.0	6.6	11	13.8	18	
59	1.36	7.6	60	0.95	6.5	54	9.0	26	56	10.9	26	26	192	5.7	
--	157	68	--	174	87	70	1.4	5.1	68	1.3	6.1	47	30.0	5.2	
						--	208	87	--	173	85	64	1.6	4.9	
												215	74		
A6			A7			A8			A9						
z	Q	P	z	Q	P	z	Q	P	z	Q	P				
2.7	112	6.7	3.8	155	7.2	3.1	95.2	6.1	2.5	70.3	6.2				
32	241	5.7	38	312	7.9	48	341	5.6	33	367	7.0				
49	37	6.3	45	10.2	20	58	40.7	4.8	40	19.9	15				
60	1.5	5.5	59	41.5	6.3	--	172	61	47	79.8	6.4				
--	171	91	--	193	87	--				217	89				

4.3. Seasonal variation of the freshwater/saltwater interface

Based on the VES-IPS inversion results before and after winter, we established the resistivity ranges used for lithological assignment (Table 2), thereby allowing the determination of the seasonal variation of the freshwater/saltwater interface.

Table 2. Resistivity and polarisability ranges used for lithological assignment, and mean values when applicable.

Q→	121	367	ates Fresh water	30	48	Gravels / conglom- erates Interface	1.0	1.6	Gravels / congo- lates Salt water	9.0	14	Clay	157	217	Schist (Substrate)
P→	5	10		40		5	10		6	12		15	25		
	6					6					22		60	90	
														75	

Although the average resistivity value for gravels/conglomerates that were saturated with freshwater was $230 \Omega\text{-m}$, this value was not considered as an initial model because it varied strongly in the area. The resistivity range of the schist substratum was also maintained. The most critical aspects of this model assignment were the low thickness levels located at increased depths, making it difficult to discriminate between the interface and intrusion zones. Regarding the polarisability values, the gravel layers showed a mean polarisability of 6 mV/V regardless of the characteristics of the saturation fluid; however, while the clay levels showed a higher mean polarisability value of 20 mV/V , the schistose substrate had a markedly higher mean polarisability value of 75 mV/V .

Using these ranges, the freshwater–saltwater interface was mapped for two seasons, i.e., before and after winter. Figure 12 shows the sections obtained from the VES-IPS, revealing the marine intrusion regression after winter and a somewhat smaller regression of the interface zone.

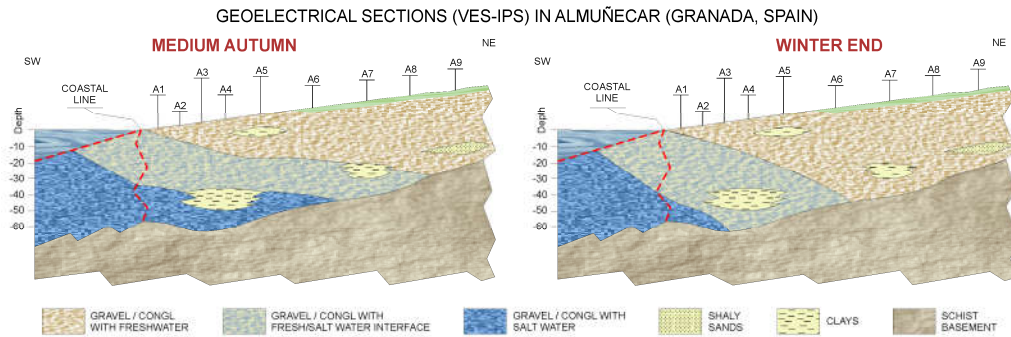


Figure 12. Sections showing the marine intrusion progress in two different seasons.

5. Discussion

The most important question to be addressed in this analysis is, when is it necessary to perform decay curve decomposition? In other words, when should the EM and residual potential effects be removed?

Cases involving EM effects with small decay times (of the order of the smallest value of the measurement range) are the ones that initially seem to require such decomposition the most. Interestingly, the cases in which the polarisation effect is low ($\sim 2 \text{ mV/V}$) are clearer.

To determine when a residual potential value needs to be eliminated, it is sufficient to obtain a value that minimises the approximation (by least squares) of a simple exponential to the data curve. If this value is negligible (i.e., $< 5\%$) compared to the cut-off value at the origin, it is not necessary to consider it.

After the first—and not definitive—removal of the residual potential, the resulting curve appears in most cases to be a simple exponential. This is because when the ratios between the parameters of the two resulting curves are less than 5, the sum of exponentials presents a behaviour very similar to that of a simple exponential; in fact, its approximation to an exponential reaches a regression coefficient of up to 0.9999. After analysing the cases studied, we found that decomposition should be conducted whenever the curve

of the logarithms of the measured values is closer to an exponential than to a straight line, i.e., whenever the ratio between the regression coefficients of both is less than 1.

We note that the discrimination that we conducted has been effective, given that the study depth was not increased (i.e., approximately 100 m), with the EM effects in the study window (i.e., 0.5–3.5 s) being lower or similar to those of polarisation. A similar result was observed in relation to the residual potential, which was below 50% of the potential value at $t = 0^+$.

Regarding the obtained residual potential V_R , we note that although it has been attributed to the possible polarisation of the electrodes, the comparative analysis of the obtained values showed the existence of a strong correlation (correlation coefficient: 0.96) between this potential and the polarisation of the medium. Even non-polarisable potential electrodes deviate from its expected behaviour by an amount proportional to the polarisation potential exerted on them by the subsurface. However, we note that there may be a relationship between V_R and ground behaviour.

Regarding the electromagnetic-effect cut-off potential V_{0EM} (and its unique time constant), it is important to note that it is futile searching for a direct interpretation of the resulting values, as this has been obtained by analysing the decay curve, whose effect is already very small and its evolution towards zero has no particular significance. Moreover, assigning only the first section of the decay curve to an induction effect in the subsurface would be problematic, as this value may include other effects, such as coupling between the cables.

Finally, we note that the developed methodology should be of interest to other researchers since it is easily applicable, especially considering that the number of measurement points used for analysing the decay curve is the minimum that can be obtained with contemporary equipment.

5.1. Error analysis

One of the main reasons for developing this work is the presence of uncertainties due to noise and errors in the measurements. These uncertainties do not allow further subdivision of the decay curve as it is done in the Laplace decomposition of the IP curves.

First, we consider the error resulting from the correct layout of the electrodes in the linear arrays. In the data of this campaign, this error, relating to the measurements at the junction points due to the increase of the MN distance (using between 2 and 4 points), was on average 15% of the resistivity value. We note that this value did not affect the distribution of the layers that we were able to obtain through the soundings.

This error likely did not affect the values of the IP decay curves at each station, as the measurement procedure was performed by adopting as valid values when the stacking process did not produce significant changes in the result. However, the polarisability values obtained from the control measurements indicated that the measured values involved uncertainties. Although the average error resulting from the values of the decay curve versus time was small (i.e., 0.05 mV/V), its relative value was not, with an average value of 4.0%. This uncertainty requires considering that selecting the segments between each pair of points on the curve may generate different decay processes corresponding only to measurement errors.

Another error requiring analysis is the one owing to the process used for curve decomposition. In this regard, the comparison between the results of the lithological section of the study areas and the position of the saline interface (by means of the columns and the water analysis of the piezometers in the study area) revealed coherence.

However, the verification of the numerical value of this error cannot be performed simply through this test, because the different values of polarisability and deduced time constants would be equally coherent within a clearly higher assignment range. In other words, errors of up to 15% in the values of these parameters would not affect the lithological and hydrochemical assignments. Therefore, to estimate this error, we compared again

the values obtained from repeated control measurements and found an average relative error of 3.9% for polarisability and 4.1% for the decay constant.

6. Conclusions

In this study, we proposed a method for processing the induced polarisation decay curve of the subsurface to obtain polarisability. Our method is more appropriate and decisive than using the conventionally obtained chargeability, since the 'average' chargeability results in loss of information regarding how different strata depolarise and the effect that certain lithologies have on EM coupling.

The results revealed the advantages of using joint geophysical techniques to avoid indeterminacy regarding the interpretation, while verifying that knowledge on polarisability constitutes an important contribution regarding the resistivity results. This combination may be of interest regarding the geological assignment of physical parameters in general, but it is even more necessary in investigations of the salinisation of coastal aquifers, both with regard to basic monitoring but also prospecting for uncontaminated levels.

The obtained seasonal variation of the frontal position of the studied marine intrusion confirms the possibilities of the referred combination, even if the thicknesses of the strata are close to the resolution capacity of the 1D techniques.

Author Contributions: Conceptualization, J.D.; methodology, J.D.; software, J.D.; validation, B.B., and L.A.; formal analysis, J.D. and M.J.M.; investigation, J.D. and B.B.; resources, J.D.; data curation, J.D. and L.A.; writing—original draft preparation, J.D. and B.B.; writing—review and editing, J.D., L.A., M.J.M. and B.B.; visualization, J.D., L.A. and M.J.M.; supervision, J.D.; project administration, J.D. and B.B.; funding acquisition, J.D. and B.B. All authors have read and agreed to the published version of the manuscript.

Funding: Please add: This research was partially funded by the Regional Government of Madrid, (CARESOIL-CM project grant number P2018/EMT-4317).

Data Availability Statement: The data presented in this study are available on request from the corresponding author. The data are not publicly available due to some special reasons.

Acknowledgments: The authors would like to acknowledge the Instituto Geológico y Minero de España (IGME) for their collaboration and help in carrying out this research.

Conflicts of Interest: The authors declare no conflict of interest.

References

1. Schlumberger, C. Etude sur la prospection électrique du sous-sol. Gauthier-Villars, **1920**.
2. Titov, K.; Komarov, V.; Tarasov, V.; Levitski, A. Theoretical and experimental study of time domain-induced polarization in water-saturated sands. *J Appl Geophy* **2002**, *50*, 417- 433. [https://doi.org/10.1016/S0926-9851\(02\)00168-4](https://doi.org/10.1016/S0926-9851(02)00168-4).
3. Angoran, Y.; Madden, T.R. Induced polarization: A preliminary study of its chemical basis. *Geophysics* **1977**, *42*(4), 788-803. <https://doi.org/10.1190/1.1440747>.
4. Grow, L.M. Induced polarization for geophysical exploration. *Lead. Edge* **1982**, *1*(1), 55-70. <https://doi.org/10.1190/1.1436726>.
5. Weller, A.; Börner, F.D. Measurements of spectral induced polarization for environmental purposes. *Environ. Geol.* **1996**, *27*(4), 329-334. <https://doi.org/10.1007/BF00766702>.
6. Weller, A.; Brune, S.; Hennig, T.; Kansy, A. Spectral induced polarization at a medieval smelting site. In Proceedings for the EEGS-ES 2000 Annual Meeting, Bochum, Germany, 2000, September.
7. Seigel, H.O. Mathematical formulation and type curves for induced polarization. *Geophysics* **1959**, *24* (3), 547-565. <https://doi.org/10.1190/1.1438625>.
8. Ward, S.H. Resistivity and Induced Polarization Methods. In *Geotechnical and Environmental Geophysics: Volume I: Review and Tutorial* (pp. 147-190). Society of Exploration Geophysicists. 1990.
9. Fiandaca, G.; Auken, E.; Christiansen, A.V.; Gazoty, A. Time-domain-induced polarization: Full-decay forward modeling and 1D laterally constrained inversion of Cole-Cole parameters. *Geophysics* **2012**, *77*(3), E213-E225. <https://doi.org/10.1190/geo2011-0217.1>.
10. Bertin, J.; Loeb, J. Transients and field behaviour in induced polarization. *Geophys. Prospect.* **1969**, *17*(4), 488-503. <https://doi.org/10.1111/j.1365-2478.1969.tb01991.x>.
11. Cole, K.S.; Cole, R.H. Dispersion and absorption in dielectrics. 1- Alternating current fields. *J. Chem. Phys.* **1941**, *9*, 341-351.
12. Pelton, W.H.; Ward, S.H.; Hallof, P.G.; Sill, W.R.; Nelson, P.H. Mineral discrimination and removal of inductive coupling with multifrequency IP. *Geophysics* **1978**, *43*, 588-609. <https://doi.org/10.1190/1.1440839>.

13. Tombs, J.M.C. The feasibility of making spectral IP measurements in the time domain. *Geoexploration* 1981, 19, 91-102. [https://doi.org/10.1016/0016-7142\(81\)90022-3](https://doi.org/10.1016/0016-7142(81)90022-3).
14. Johnson, I.M. Spectral induced polarization parameters as determined through time-domain measurements. *Geophysics* 1984, 49, 1993-2003. <https://doi.org/10.1190/1.1441610>.
15. Duckworth, K.; Calver, H.T. An examination of the relationship between time domain integral chargeability and the Cole-Cole impedance model. *Geophysics* 1995, 60 (41), 1249-1252. <https://doi.org/10.1190/1.1443855>.
16. Rubio, F.M.; Plata, J.L. Nueva campaña geofísica en el acuífero aluvial del río Verde (Almuñecar, Granada). *Boletín Geológico y Min.* 2002, 113 (1): 57-69. ISSN: 0366-0176.
17. Hönig, M.; Tezkan, B. 1-D and 2-D Cole-Cole inversion of time domain induced polarization data. *Geophys. Prospect.* 2007, 55, 117-133. <https://doi.org/10.1111/j.1365-2478.2006.00570.x>.
18. Dahlin, T.; Leroux, V.; Nissen, J. Measuring techniques in induced polarisation imaging. *J Appl Geophy* 2002, 50, 279-298. [https://doi.org/10.1016/S0926-9851\(02\)00148-9](https://doi.org/10.1016/S0926-9851(02)00148-9).
19. Ogilvy, R.D.; Meldrum, P.I.; Kuras, O.; Wilkinson, P.B.; Chambers, J.E.; Sen M.; Pulido-Bosch, A.; Gisbert, J.; Jorreto, S.; Frances, I.; Tsurlos, P. Automated monitoring of coastal aquifers with electrical resistivity tomography. *Near Surf. Geophys.* 2009, 367-375. <https://doi.org/10.3997/1873-0604.2009027>.
20. Bleil, D.F. Induced polarization: A method of geophysical prospecting, *Geophysics* 1953, 18, 636-661. <https://doi.org/10.1190/1.1437917>.
21. Frische, R.H.; Von Buttlar, H. A Theoretical Study of Induced Electrical Polarization. *Geophysics* 1957, 22 (3), 688-706. <https://doi.org/10.1190/1.1438404>.
22. Wait, J.R. Discussions on a theoretical study of induced electrical polarization. *Geophysics* 1958, 23, 144-154.
23. Marshall, D.J.; Madden, T.R. Induced polarization, a study of its causes. *Geophysics* 1959, 24, 790-816. <https://doi.org/10.1190/1.1438659>.
24. Vacquier, V.; Holmes, C.R.; Kintzinger, P.R.; Lavergne, M. Prospecting for ground water by induced electrical polarization. *Geophysics* 1957, 22(3), 660-687. <https://doi.org/10.1190/1.1438402>.
25. Sandberg, S.K. Examples of resolution improvement in geoelectrical soundings applied to groundwater investigations. *Geophys. Prospect.* 1993, 41(2), 207-227. <https://doi.org/10.1111/j.1365-2478.1993.tb00866.x>.
26. Slater, L.D.; Lesmes, D. IP interpretation in environmental investigations. *Geophysics* 2002, 67(1), 77-88. <https://doi.org/10.1190/1.1451353>.
27. Shevnin, V.; Delgado-Rodríguez, O.; Mousatov, A.; Ryjov, A. Estimation of soil hydraulic conductivity on clay content, determined from resistivity data. In 19th EEGS Symposium on the Application of Geophysics to Engineering and Environmental Problems (pp. cp-181). European Association of Geoscientists & Engineers, 2006, April. <https://doi.org/10.3997/2214-4609-pdb.181.149>.
28. Weller, A.; Slater, L.; Nordsiek, S. On the relationship between induced polarization and surface conductivity: Implications for petrophysical interpretation of electrical measurements. *Geophysics* 2013, 78(5), D315-D325. <https://doi.org/10.1190/geo2013-0076.1>.
29. Brandes, I.; Acworth, R.I. Intrinsic Negative Chargeability of Soft Clays. ASEG Extended Abstracts 2003,(2), 1-4. <https://doi.org/10.1071/ASEG2003ab017>.
30. Slater, L.; Ntarlagiannis, D.; Wishart, D. On the relationship between induced polarization and surface area in metal-sand and clay-sand mixtures. *Geophysics* 2006, 71(2), A1-A5. [10.1190/1.2187707](https://doi.org/10.1190/1.2187707).
31. Dahlin, T.; Loke, M.H. Negative apparent chargeability in time-domain induced polarisation data. *J Appl Geophy* 2015, 123, 322-332. <https://doi.org/10.1016/j.jappgeo.2015.08.012>.
32. Börner, F.; Weller, A.; Schopper, J. Evaluation of Transport and Storage Properties in the Soil And Groundwater zone from Induced Polarization Measurements. *Geophys. Prospect.* 1996, 44 (4), 583-601. <https://doi.org/10.1111/j.1365-2478.1996.tb00167.x>.
33. Slater, L.D.; Glaser, D.R.; Controls on induced polarization in sandy unconsolidated sediments and application to aquifer characterization. *Geophysics* 2003, 68, 1547-1588. <https://doi.org/10.1190/1.1620628>.
34. Scott, J.B.T.; Barker, R.D. Determining pore-throat size in Permo-Triassic sandstones from low-frequency electrical spectroscopy. *Geophys. Res. Lett.* 2003, vol. 30, No. 9, 1450. <https://doi.org/10.1029/2003GL016951>.
35. Binley, A.; Slater, L.D.; Fukes, M.; Cassiani, G. Relationship between spectral induced polarization and hydraulic properties of saturated and unsaturated sandstone. *Water Resour. Res.* 2005, 41, W12417. <https://doi.org/10.1029/2005WR004202>.
36. Worthington, P.F.; Collar, F.A. Relevance of induced polarization to quantitative formation evaluation. *Mar Pet Geol* 1984, 1(1), 14-26. [https://doi.org/10.1016/0264-8172\(84\)90117-X](https://doi.org/10.1016/0264-8172(84)90117-X).
37. Klein, J.D.; Sill, W.R.. Electrical properties of artificial claybearing sandstone, *Geophysics* 1982, 47, 1593-1605. <https://doi.org/10.1190/1.1441310>.
38. Vinegar, H.J.; Waxman, M.H. Induced polarization of shaly sands: *Geophysics* 1984, 49, 1267-1287.
39. Vanhala, H.; Peltoniemi, M. Spectral IP studies of Finnish ore prospects. *Geophysics* 1992, 57, 1545-1555.
40. Roy, K.K.; Bhattacharyya, J.; Mukherjee, K.K.; Resistivity and induced polarisation sounding for location of saline water pockets. *Explor. Geophys.* 1995, 25, 207-211. <https://doi.org/10.1071/EG994207>.
41. Martinho, E.; Almeida, F.; Senos, M.J. An experimental study of organic pollutant effects on time domain induced polarization measurements. *J Appl Geophy* 2006, 60, 27-40. <https://doi.org/10.1016/j.jappgeo.2005.11.003>.
42. Seara, J. L.; Granda, A. Interpretation of IP time domain/resistivity soundings for delineating sea-water intrusions in some coastal areas of the northeast of Spain. *Geoexploration* 1987, 24(2), 153-167. [https://doi.org/10.1016/0016-7142\(87\)90089-5](https://doi.org/10.1016/0016-7142(87)90089-5).

43. Martinho, E.; Almeida, F.; Matias, M.J. Time-domain induced polarization in the determination of the salt/freshwater interface (Aveiro-Portugal). Groundwater and saline intrusion" (L. Araguás, E. Custodio & M. Manzano, Ed.), 385-393. **2004**.

44. Sastry, R.G.; Tesfakiros, H.G. Neural network based interpretation algorithm for combined induced polarization and vertical electrical soundings of coastal zones. *J. Environ. Eng. Geophys* **2006**, 11(3), 197-211. <https://doi.org/10.2113/JEEG11.3.197>.

45. Attwa, M.; Günther, T.; Grinat, M.; Binot, F. Evaluation of DC, FDEM and SIP resistivity methods for imaging a perched saltwater and shallow channel within coastal tidal sediments, Germany. *J Appl Geophys* **2011**, 75: 656-670.

46. Attwa, M.; Ali, H. Resistivity Characterization of Aquifer in Coastal Semi-arid Areas: An Approach for Hydrogeological Evaluation. *Groundwater in the Nile Delta* **2018**, 213-233. https://doi.org/10.1007/698_2017_210.

47. Aladejana, J.A.; Kalin, R.M.; Sentenac, P.; Hassan, I. Hydrostratigraphic characterisation of shallow coastal aquifers of Eastern Dahomey Basin, S/W Nigeria, using integrated hydrogeophysical approach; implication for saltwater intrusion. *Geosciences* **2020**, 10(2), 65. <https://doi.org/10.3390/geosciences10020065>.

48. Attwa, M.; El Mahmoudi, A.; Elshennawey, A.; Günther, T.; Altahrany, A.; Mohamed, L. Soil Characterization Using Joint Interpretation of Remote Sensing, Resistivity and Induced Polarization Data along the Coast of the Nile Delta. *Nat. Resour. Res.* **2021**, 30(5), 3407-3428. <https://doi.org/10.1007/s11053-021-09883-9>.

49. Karabulut, S.; Cengiz, M.; Balkaya, Ç.; Aysal, N. Spatio-Temporal Variation of Seawater Intrusion (SWI) inferred from geophysical methods as an ecological indicator; A case study from Dikili, NW Izmir, Turkey. *J Appl Geophys* **2021**, 189, 104318. <https://doi.org/10.1016/j.jappgeo.2021.104318>.

50. Aal, G.A.; Slater, L. D.; Atekwana, E.A. Induced-polarization measurements on unconsolidated sediments from a site of active hydrocarbon biodegradation. *Geophysics* **2006**, 71(2), H13-H24, doi:10.1190/1.2187760.

51. Ustra, A.; Slater, L.; Ntarlagiannis, D.; Elis, V. Spectral induced polarization (SIP) signatures of clayey soils containing toluene. *Near Surf. Geophys.* **2012**, 10(6), 503-515. <https://doi.org/10.3997/1873-0604.2012015>.

52. Flores Orozco, A.F.; Kemna, A.; Oberdörster, C.; Zschornack, L.; Leven, C.; Dietrich, P.; Weiss, H. Delineation of subsurface hydrocarbon contamination at a former hydrogenation plant using spectral induced polarization imaging. *J. Contam. Hydrol.* **2012**, 136, 131-144. <https://doi.org/10.1016/j.jconhyd.2012.06.001>.

53. Gazoty, A.; Fiandaca, G.; Pedersen, J.; Auken, E.; Christiansen, A.V. Mapping of landfills using time domain spectral induced polarization data: the Eskelund case study. *Near Surf. Geophys.* **2012**, 10(6), 575-586. <https://doi.org/10.3997/1873-0604.2012046>.

54. Johansson, S.; Fiandaca, G.; Dahlin, T. Influence of non-aqueous phase liquid configuration on induced polarization parameters: Conceptual models applied to a time-domain field case study. *J Appl Geophys* **2015**, 123, 295-309. <https://doi.org/10.1016/j.jappgeo.2015.08.010>.

55. Ntarlagiannis, D.; Robinson, J.; Soupios, P.; Slater, L. Field-scale electrical geophysics over an olive oil mill waste deposition site: Evaluating the information content of resistivity versus induced polarization (IP) images for delineating the spatial extent of organic contamination. *J Appl Geophys* **2016**, 135, 418-426. <https://doi.org/10.1016/j.jappgeo.2016.01.017>.

56. Frid, V.; Sharabi, I.; Frid, M.; Averbakh, A. Leachate detection via statistical analysis of electrical resistivity and induced polarization data at a waste disposal site (Northern Israel). *Environ. Earth Sci.* **2017**, 76(6), 1-18. 10.1007/s12665-017-6554-4.

57. Luo, Y.; Zhang, G. Theory and Application of Spectral Induced Polarization. Geophysical Monograph Series No. 8. Society of Exploration Geophysicists (USA). **1998**.

58. Xiang, J.N.B.; Jones, D.; Cheng, D.; Schlindwein, F.S. A new method to discriminate between a valid IP response and EM coupling effects. *Geophys. Prospect.* **2002**, 50, 566-576. <https://doi.org/10.1046/j.1365-2478.2002.00344.x>.

59. Tong, M.; Li, L.; Wang, W.; Yizhong Jiang, Y. A time-domain induced-polarization method for estimating permeability in a shaly sand reservoir. *Geophys. Prospect.* **2006**, 54, 623-631. <https://doi.org/10.1111/j.1365-2478.2006.00568.x>.

60. Johnston, D.C. Stretched exponential relaxation arising from a continuous sum of exponential decays. *Phys. Rev. B* **2006**, 74(18), 184430. <https://doi.org/10.1103/PhysRevB.74.184430>.

61. Kang, S.; Oldenburg, D.W. Inversions of time-domain spectral induced polarization data using stretched exponential. *Geophys. J. Int.* **2019**, 219(3), 1851-1865. <https://doi.org/10.1093/gji/ggz401>.

62. Kang, S.; Oldenburg, D.W.; Heagy, L.J. Detecting induced polarisation effects in time-domain data: a modelling study using stretched exponentials. *Explor. Geophys.* **2020**, 51(1), 122-133. <https://doi.org/10.1080/08123985.2019.1690393>.

63. Ghosh, D.P. The application of linear filter theory to the direct interpretation of geoelectrical resistivity sounding measurements. *Geophys. Prospect.* **1971**, 19(2), 192-217. <https://doi.org/10.1111/j.1365-2478.1971.tb00593.x>.

64. Roy, A.; Poddar, M. A simple derivation of Seigel's time domain induced polarization formula. *Geophys. Prospect.* **1981**, 29, 432-437. <https://doi.org/10.1111/j.1365-2478.1981.tb01023.x>.

65. Benavente, J.; Terrón, E. Características hidroquímicas del acuífero aluvial litoral de Castell de Ferro (Granada). III Simposio de Hidrogeología. Madrid. **1983**.

66. Fernández-Rubio, R. Proceso de salinización-desalinización en el acuífero costero del Río Verde (Almuñécar-Granada). Simposio El Agua en Andalucía. Granada. **1986**.

67. Díaz-Curiel, J.; Martín Sánchez, D.; Maldonado Zamora, A.; Gómez Martos, M. Red de control σ/T para el estudio de intrusión marina en Almuñécar (Granada). *Boletín Geológico y Min.* **1995**, 106(4), 358-372. Instituto Geológico y Minero de España (<http://www.igme.es/internet/pr...>). ISSN 0366-0176.